Surface-emitting quantum cascade lasers with metallic photonic-crystal resonators

Gangyi Xu,[1,a)] Virginie Moreau,[1] Yannick Chassagneux,[1] Adel Bousseksou,[1] Raffaele Colombelli,[1,b)] G. Patriarche,[2] G. Beaudoin,[2] and I. Sagnes[2]
[1]*Institut d'Electronique Fondamentale, Université Paris Sud, UMR8622 CNRS, 91405 Orsay, France*
[2]*Laboratoire de Photonique et Nanostructures, LPN/CNRS, Route de Nozay, 91460 Marcoussis, France*

(Received 20 January 2009; accepted 26 March 2009; published online 1 June 2009)

Surface emitting photonic-crystal quantum cascade lasers operating at $\lambda \approx 7.3$ μm are demonstrated. The photonic crystal resonator is written solely on the top metallization layer. The mismatch between the modes supported by metallized and nonmetallized regions yields enough optical feedback to achieve laser action. The devices exhibit single-mode emission with a side mode suppression ratio of ≈ 20 dB, the wavelength is lithographically tunable across a range of almost 70 cm^{-1}, and the radiation is emitted from the surface. The maximum operating temperature is 220 K. The divergence of the output beam, which is doughnut-shaped, is approximately 9°. © *2009 American Institute of Physics*. [DOI: 10.1063/1.3143652]

The development of quantum cascade lasers (QCLs) in recent years has made them powerful semiconductor laser sources for the mid- and far-infrared spectral regions.[1–4] However, for the development of arrays of high brilliance sources,[4] QCLs with single-mode surface-emission and low output divergence are highly desirable. Due to the intrinsic transverse magnetic polarization, the fabrication of surface emitting QCLs is not an immediate task. A diffracting element, second-order distributed feedback (DFB) grating, or a two-dimensional (2D) photonic crystal (PC) pattern, needs to be embedded monolithically in the QCL.[5–9] These two approaches are similar: in-plane optical feedback is obtained via the periodic index variation in the waveguide, while surface emission is obtained by second-order Bragg diffraction. Compared to the second order DFB, the advantage of 2D PC structures is the flexibility that the 2D geometry provides for device spectral and spatial engineering.[10–13]

Surface emission PC QCLs operating on band-edge states were first demonstrated in the midinfrared.[8] The crucial issue is the elevated index contrast needed for strong optical feedback, which in Ref. 8 was obtained via etching of air holes through the laser active region and into the substrate. This approach yields high index contrasts (3.4–1 in Ref. 8), but it is technologically heavy. Recently, electrically pumped PC lasers operating in the terahertz range were demonstrated with controllable far-field emission, in which the PC resonator is *written* in the top metallization.[9] No semiconductor etching is necessary, thus simplifying the technology. The extreme mode confinement typical of terahertz metal-metal waveguides results in a reasonably high effective-index contrast (3.6–2.8, approximately).

In this paper, we extend this simpler approach to laser devices operating in the midinfrared and employing surface-plasmon waveguides.[14] The laser structure (sample E-InP281) is based on an $In_{0.53}Ga_{0.47}As/Al_{0.48}In_{0.52}As$ lattice matched to InP substrate. The active region contains 50 active-region/injector stages with the nominal lasing transition at $\lambda = 7.5$ μm. Details of the growth are given in Ref. 15. The device process started by defining the PC pattern by e-beam lithography, using a two-layer resist mask (PMMA and FOx12), followed by metal evaporation (Ti/Au, 3/80 nm) and liftoff. A schematics and a scanning electron microscope (SEM) image of a typical device are presented in Figs. 1(a) and 1(b), respectively. The Ti/Au film served simultaneously as surface plasmon carrying layer and as contact layer for current injection. In order to overlap the PC modes with the material gain peak, the lattice period (a) was lithographically varied from 2.54 to 2.68 μm. Four different values of r/a (0.1, 0.2, 0.3, and 0.4) were chosen, where r is the radius of air holes. After defining the top metallic contact size and shape by wet chemical etching, irregular mesa cavities were wet etched down to the InP substrate for current confinement. The irregular cavity, shown in Fig. 1(b), was implemented to avoid the excitation of whispering-gallery-like modes.[9] The cavity sidewalls and the mesa top edges were covered by 200-nm-thick Si_xN_y. The top electrode was formed by evaporating a Ti/Au layer, which surrounded and contacted the edge of the PC pattern. Substrate thinning down to 250 μm, polishing, and back contact deposition

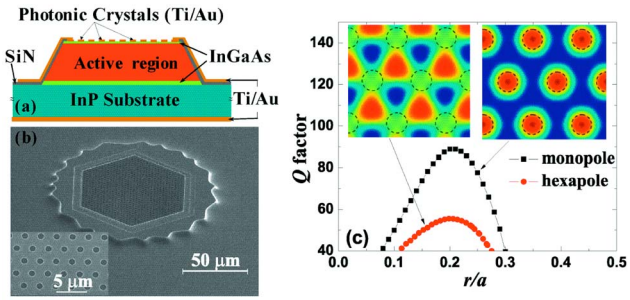

FIG. 1. (Color online) (a) Schematic cross section of a device. (b) SEM image of a typical device. Inset: close-up of the photonic-lattice implemented only in the metallic top layer. (c) 2D FDTD calculation of the photonic-crystal resonator Q-factor—for the hexapole and the monopole modes—as a function of r/a. The number of photonic-crystal periods from the center of the resonator is 20. The insets represent the electromagnetic field distributions (E_z component, orthogonal to the plane of the PC) for the hexapole (left) and monopole modes (right). The field is sampled inside the active region, below the PC. The dashed circles mark the edges of the air holes.

a)Electronic mail: gangyi.xu@u-psud.fr.
b)Electronic mail: raffaele.colombelli@u-psud.fr.

concluded the processing. The devices were then mounted in a cryostat for device characterization.

In the absence of a strong mode confinement, the index contrast is low.[15] One-dimensional (1D) transfer-matrix calculations indicate that the effective indices of the mode guided at the metal-semiconductor interface and at the air-semiconductor interface are 3.24 and 3.14, respectively. However, the profile mismatch between these two modes is significant, because the metal-semiconductor interface tends to bind the electromagnetic field, while the air-semiconductor interface repels it into the active core. This significant mismatch, in combination with a careful design of the PC resonator, is exploited here to obtain sufficient optical feedback.

The hexagonal PC pattern [Fig. 1(b)] contains a triangular lattice of air holes in the top metallic contacts. We exploit the states at the Γ point of the photonic band structure, which have small group velocity and high photonic density, to obtain strong optical feedback. The complex eigenfrequencies and the electromagnetic field of the predominant TM modes at the Γ point were calculated by solving the three-dimensional Helmholtz equation with Bloch periodic boundary conditions. Six states exist at the Γ-point in correspondence of the second-order Bragg diffraction condition ($a/\lambda \approx 0.35$, with λ as the emission wavelength in free space). Only two of them exhibit relatively low losses (α) and are of interest. They are the hexapole ($\alpha=27.8\ \mathrm{cm}^{-1}$, $a/\lambda=0.356$) and the monopole mode ($\alpha=9.5\ \mathrm{cm}^{-1}$, $a/\lambda=0.361$), whose electromagnetic field distribution is reported in the inset of Fig. 1(c). The calculated losses of the other modes are $\geq 40\ \mathrm{cm}^{-1}$.

To estimate the quality (Q) factor of the two modes, we performed 2D finite-difference time-domain (FDTD) simulations by using the effective indices inferred from the 1D calculation.[16] Figure 1(c) shows the calculated Q-factor as a function of r/a for the hexapole and monopole modes, respectively. The figure demonstrates that the Q-factor is extremely sensitive to the r/a value. For each mode, the Q-factor reaches its maximum for $r/a \approx 0.2$ and decreases rapidly when r/a deviates from 0.2. The calculation also shows that the Q-factor of the monopole mode is higher than that of the hexapole mode. Note that the monopole mode is typically inactive in standard deep-etched PC devices, since a large part of the electromagnetic field is in the holes with no optical gain. The possibility of operating on a monopole mode is instead possible for our structures (no active material is removed), representing an additional degree of freedom.

Figure 2 shows the lasing spectra of several devices with the same r/a ratio (0.2), same PC dimension (150 μm), but different lattice periods a. Here, PC dimension means the diameter of the circumscribed circle of the hexagonal PC pattern. The spectra were measured at a temperature of 78 K. Single mode emission with a side-mode suppression ratio of ≈20 dB was observed for all the devices. The emission wavelengths tune linearly with the lattice period, corresponding to a normalized frequency value $a/\lambda=0.365$, in good agreement with the calculated values of the hexapole and monopole modes. By lithographically tuning a, the emission frequency is tunable in a wide range of $\approx 70\ \mathrm{cm}^{-1}$ (350 nm in wavelength). The emission is always single mode for all the injected currents, operation temperatures, and photonic

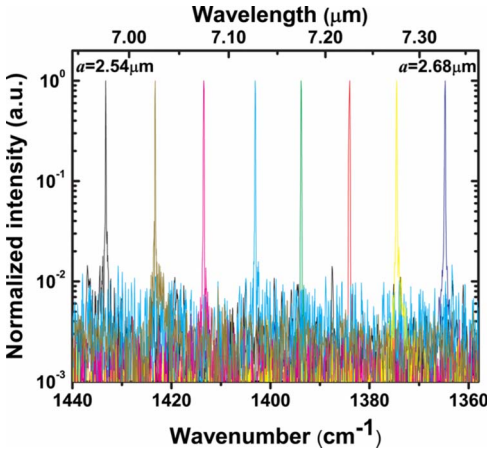

FIG. 2. (Color online) Lasing spectra for several devices with the same r/a ratio (0.2) and with different lattice periods a (from 2.54 to 2.68 μm, in steps of 20 nm). The spectra were measured at a heat sink temperature of 78 K. The lasers were operated in pulsed mode, with a repetition rate of 84 kHz and pulse widths of 20 ns.

lattice periods explored, demonstrating a strong 2D DFB. The measurements confirm that the laser resonance is very sensitive to the r/a value. For the other tested values of r/a (0.1, 0.3, 0.4), no lasing (and not even resonances in the electroluminescence spectra) was observed.

Figure 3 shows the light-current-voltage (L-I-V) characteristics of a typical device measured at different temperatures. The threshold current density (J_{th}) at 78K is 2.9 $\mathrm{kA/cm}^2$ and it increases to 6.7 $\mathrm{kA/cm}^2$ at 220 K, the maximum operating temperature (T_{max}). To account for current dispersion effects,[17] the full device top surface is considered for the calculation of J_{th}. The peak output power reaches 43 mW at 77 K and it decreases to 0.2 mW at 220 K. We note that for standard ridge QCLs fabricated from the same epitaxial material, the J_{th} at 77 K and T_{max} are 2.5 $\mathrm{kA/cm}^2$ and 260 K, respectively. The performance degradation is possibly caused by the nonoptimized design of the PC, especially the r/a value, which was not fine tuned in this work. The inset of Fig. 3 shows the value of J_{th} as a function of the lattice period. It suggests that J_{th} reaches its minimum when the wavelength of the PC mode overlaps with the gain peak.

Figure 4 shows the far-field emission patterns of two devices with the same a (2.66 μm) and r/a (0.2), but dif-

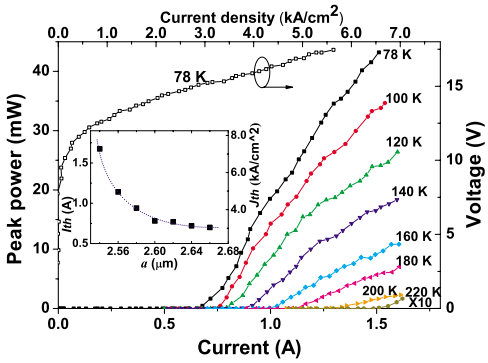

FIG. 3. (Color online) L-I-V characteristics of a laser (PC dimension 150 μm, $a=2.66$ μm, $r/a=0.20$) for different heat sink temperatures. The inset reports the threshold currents of lasers with different lattice periods a (PC dimension 150 μm, $r/a=0.20$), measured at 78 K.

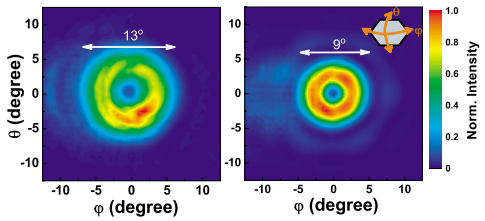

FIG. 4. (Color online) Far-field emission patterns of devices with $a=2.66$ μm and $r/a=0.2$, measured at 78 K in pulsed mode. The repetition rate was 84 kHz and the pulse width was 50 ns. Left: when the PC dimension is 100 μm, the divergence angle is 13°. Right: When the PC dimension is 150 μm, the divergence angle is 9°.

ferent PC dimensions (100 and 150 μm). The far-field patterns have a "doughnut" shape, as expected from devices operating on photonic-lattice band-edge states without phase shifters.[18] Figure 4 shows that the narrow angular spread decreases from 13° to 9° when the PC dimension increases from 100 to 150 μm, demonstrating that the laser mode is spatially delocalized.[8] The identification of the PC is a mode beyond the scope of this article. However, the simulations reported in Fig. 1(c) suggest that the monopole mode is the most probable candidate for its higher Q-factor.

In summary, we reported surface emitting midinfrared PC QCLs with single mode, angularly narrow surface emission, and a large lithographically tunable range of emission wavelengths. The results demonstrate that for midinfrared devices strong optical feedback can be obtained by writing the PC on the top metallization layer. Future works will target key issues that could make these devices interesting for applications: improvement of T_{max}, the maximization of the output power, and the full control of the far-field emission pattern.

We thank B. Dagens, B. Vilquin, and F. Julien for help and discussions. The device fabrication was performed at the nanocenter CTU-IEF-Minerve, which was partially funded by the "Conseil Général de l'Essonne." This work is supported by a EURYI scheme award, see www.esf.org/euryi, and the French National Research Agency (Grant No. ANR-06-NANO-047 "MetalGuide").

[1] R. Kohler, A. Tredicucci, F. Beltram, H. E. Beere, E. H. Linfield, A. G. Davies, D. A. Ritchie, R. C. Iotti, and F. Rossi, Nature (London) **417**, 156 (2002).
[2] A. Lyakh, C. Pflügl, C. Diehl, Q. J. Wang, F. Capasso, X. J. Wang, J. Y. Fan, T. Tanbun-Ek, R. Maulini, A. Tsekoun, R. Go, and C. K. N. Patel, Appl. Phys. Lett. **92**, 111110 (2008).
[3] S. Slivken, A. Evans, W. Zhang, and M. Razeghi, Appl. Phys. Lett. **90**, 151115 (2007).
[4] B. G. Lee, M. A. Belkin, R. Audet, J. MacArthur, L. Diehl, C. Pflugl, F. Capasso, D. C. Oakley, D. Chapman, A. Napoleone, D. Bour, S. Corzine, G. Hofler, and J. Faist, Appl. Phys. Lett. **91**, 231101 (2007).
[5] E. Mujagić, L. K. Hoffmann, S. Schartmer, M. Nobile, W. Schrenk, M. P. Semtsiv, M. Wienold, W. T. Masselink, and G. Strasser, Appl. Phys. Lett. **93**, 161101 (2008).
[6] C. Pflügl, M. Austerer, W. Schrenk, S. Golka, G. Strasser, R. P. Green, L. R. Wilson, J. W. Cockburn, A. B. Krysa, and J. S. Roberts, Appl. Phys. Lett. **86**, 211102 (2005).
[7] J. A. Fan, M. A. Belkin, F. Capasso, S. Khanna, M. Lachab, A. G. Davies, and E. H. Linfield, Opt. Express **14**, 11672 (2006); S. Kumar, B. S. Williams, Q. Qin, A. W. M. Lee, Q. Hu, and J. L. Reno, *ibid.* **15**, 113 (2007).
[8] R. Colombelli, K. Srinivasan, M. Troccoli, O. Painter, F. Gmachl, D. M. Tennant, A. Sergent, D. L. Sivco, A. Y. Cho, and F. Capasso, Science **302**, 1374 (2003).
[9] Y. Chassagneux, R. Colombelli, W. Maineult, S. Barbieri, H. Beere, D. Ritchie, S. P. Khanna, E. H. Linfield, and A. G. Davies, Nature (London) **457**, 174 (2009).
[10] M. Bahriz, V. Moreau, R. Colombelli, O. Crisafulli, and O. Painter, Opt. Express **15**, 5948 (2007).
[11] O. Painter, R. K. Lee, A. Scherer, A. Yariv, J. D. O'Brien, P. D. Dapkus, and I. Kim, Science **284**, 1819 (1999).
[12] E. Miyai, K. Sakai, T. Okano, W. Kunishi, D. Ohnishi, and S. Noda, Nature (London) **441**, 946 (2006).
[13] K. Srinivasan and O. Painter, Opt. Express **10**, 670 (2002).
[14] M. Bahriz, V. Moreau, J. Palomo, R. Colombelli, D. A. Austin, J. W. Cockburn, L. R. Wilson, A. B. Krysa, and J. S. Roberts, Appl. Phys. Lett. **88**, 181103 (2006).
[15] A. Bousseksou, V. Moreau, R. Colombelli, C. Sirtori, G. Patriarche, O. Mauguin, L. Largeau, G. Beaudoin, and I. Sagnes, Electron. Lett. **44**, 807 (2008).
[16] A. Farjadpour, D. Roundy, A. Rodriguez, M. Ibanescu, P. Bermel, J. D. Joannopoulos, S. G. Johnson, and G. Burr, Opt. Lett. **31**, 2972 (2006).
[17] V. Moreau, M. Bahriz, R. Colombelli, R. Perahia, O. Painter, L. R. Wilson, and A. B. Krysa, Opt. Express **15**, 14861 (2007).
[18] G. Vecchi, F. Raineri, I. Sagnes, A. Yacomotti, P. Monnier, T. J. Karle, K.-H. Lee, R. Braive, L. Le Gratiet, S. Guilet, G. Beaudoin, A. Talneau, S. Bouchoule, A. Levenson, and R. Raj, Opt. Express **15**, 7551 (2007).